Identification and Characterization of a B-Raf Kinase Alpha Helix Critical for the Activity of MEK Kinase in MAPK Signaling

Diep Nguyen[1], Linda Yingqi Lin[1], Jeffrey O. Zhou[1], Emily Kibby[1], Twan W. Sia[1], Tiara D. Tillis[1], Narine Vapuryan[1], Ming-Ray Xu[1], Rajiv Potluri[1], YongJoon Shin[1], Elizabeth A. Erler[1], Naomi Bronkema[1], Daniel J. Boehlmer[1], Christopher D. Chung[1], Caroline Burkhard[1], Michael Grasso[2,3], Lucila A. Acevedo[3,4], Ronen Marmorstein[2,3,4], Daniela Fera[1]

[1]Department of Chemistry and Biochemistry, Swarthmore College, Swarthmore, PA 19081

[2]Department of Chemistry, University of Pennsylvania, Philadelphia, PA, 19104

[3]Department of Biochemistry and Biophysics, Perelman School of Medicine, University of Pennsylvania, Philadelphia, PA, 19104

[4]Abramson Family Cancer Research Institute, Perelman School of Medicine, University of Pennsylvania, Philadelphia, PA, 19104

*** Correspondence:**

Daniela Fera

dfera1@swarthmore.edu

Abstract

In the MAPK pathway, an oncogenic V600E mutation in B-Raf kinase causes the enzyme to be constitutively active, leading to aberrantly high phosphorylation levels of its downstream effectors, MEK and ERK kinases. The V600E mutation in B-Raf accounts for more than half of all melanomas and ~3% of all cancers and many drugs target the ATP-binding site of the enzyme for its inhibition. Since B-Raf can develop resistance against these drugs and such drugs can induce paradoxical activation, drugs that target allosteric sites are needed. To identify other potential drug targets, we generated and kinetically characterized an active form of B-Raf^{V600E} expressed using a bacterial expression system. In doing so, we identified an alpha helix on B-Raf, found at the B-Raf-MEK interface, that is critical for their interaction and the oncogenic activity of B-Raf^{V600E}. We performed binding experiments between B-Raf mutants and MEK using pull downs and biolayer interferometry, and assessed phosphorylation levels of MEK as well as its downstream target ERK to show that mutating certain residues on this alpha helix is detrimental to binding and downstream activity. Our results suggest that this B-Raf alpha helix binding site on MEK could be a site to target for drug development to treat B-Raf^{V600E}-induced melanomas.

Introduction

The mitogen-activated protein kinase (MAPK) pathway plays an important role in cellular growth and differentiation through the downstream effects of its activation. As such, its dysregulation leads to a number of cancers, in many cases because protein mutations lead to constitutive activity and uncontrolled cell proliferation [1-3]. This pathway is initiated by growth factor binding to a receptor at the cell membrane, thereby activating a number of adaptor molecules which in turn activate Ras. Active Ras binds to guanosine triphosphate (GTP), which allows it to associate with the Ras binding domain of Raf, a serine/threonine kinase, at the membrane [4-6]. The binding of Ras to the N-terminal domain of Raf causes a conformational change in Raf that frees the C-terminal kinase domain from the N-terminal domain [7]. Raf exists in the cytosol as a quiescent Raf-MEK complex [8], and Ras binding promotes formation of heterotetramers (MEK—B-Raf—B/C-Raf—MEK). This activation leads to the phosphorylation of MEK1/2, downstream activation of ERK1/2, and cell proliferation at later stages of the MAPK pathway [9].

Raf kinases have three distinct isoforms in humans – A-Raf, B-Raf, and C-Raf. The B-Raf isoform has been shown to be particularly susceptible to mutation, with over half of melanomas containing activating B-Raf mutations, of which over 90% involve a particular mutant, B-Raf^{V600E} [10, 11]. This mutation renders B-Raf constitutively active, independent of both Ras activation and formation of tetrameric complexes. B-Raf^{V600E} mutants are locked in an active conformation because the negatively charged glutamate residue mimics phosphorylation of the activation loop, which releases its inhibitory interaction with the ATP-binding domain, found between the N- and C-lobes of the kinase domain [12]. The B-Raf isoform also has the strongest

activity towards MEK [13]. B-Raf^{V600E} mutants mediate unregulated phosphorylation of two conserved residues in the MEK activation loop, S218 and S222 of MEK1 (or S222 and S226 of MEK2) [14-16]. This phosphorylation increases MEK activity, which leads to the binding, phosphorylation, and activation of ERK. ERK1 gets phosphorylated on T202/Y204 and ERK2 gets phosphorylated on T183/Y185 [17, 18]. Activated ERK can translocate to the nucleus to phosphorylate and regulate transcription factors resulting in changes in gene expression [19]. Some ERK substrates are also found in the cytoplasm and other organelles [20].

Drug discovery efforts against oncogenic B-Raf, mainly B-Raf^{V600E}, have largely focused on targeting the ATP-binding pocket and several (e.g. vemurafenib and dabrafenib) have achieved approval by the FDA for treatment of some B-Raf-mutated melanomas [10, 21, 22]. However, acquired resistance to these competitive inhibitors and paradoxical activation in cells harboring wild-type B-Raf or mutants other than B-Raf^{V600E} show the need for allosteric inhibitors and combination therapies [23-26]. The B-Raf-MEK interface represents a potential target for allosteric inhibition of B-Raf activity as this binding interaction is critical to the phosphorylation of MEK and the activation of downstream targets [23, 27]. Mutational studies using the available crystal structure of the complex can provide site-specific information about particular surfaces that may be promising drug targets due to their role in enhancing or inhibiting the B-Raf-MEK interaction [8].

Many studies of B-Raf rely on the use of Sf9 insect cells for expression since it has been well established to produce the active enzyme [28]. Mammalian cells have also been used, but yields are often low [29, 30]. A recent report had modified the B-Raf kinase domain by the introduction of 16

mutations to improve soluble protein expression using bacterial cells for X-ray crystallographic studies [31]. Unfortunately, expression of the B-Raf^{V600E} kinase domain with these 16 surface mutations (called B-Raf^{16mut}) yielded an inactive enzyme despite no mutations of key catalytic residues, and the ability to bind ATP was intact (though its K_m was not determined). Using B-Raf^{16mut} expressed in bacteria as a starting point, we generated an active B-Raf construct that can be produced in *E. coli*. We further identified and characterized an α-helix (residues 661-671) in B-Raf that we showed is critical for the interaction with MEK. This site of interaction offers a new target for therapeutics against B-Raf^{V600E}-induced malignancies.

Materials and Methods

Expression and Purification of Proteins

DNA encoding the B-Raf kinase domain residues 448-723 containing 16 solubilizing mutations in the C-lobe (I543A, I544S, I551K, Q562R, L588N, K630S, F667E, Y673S, A688R, L706S, Q709R, S713E, L716E, S720E, P722S, and K723G) was ordered from Epoch Biolabs. This construct was cloned into a pRSF vector with an N-terminal GST tag and a TEV protease cleavage site between the tag and protein. DNA encoding the B-Raf kinase domain residues 442-724 was used as a template and cloned into a Pfastbac dual vector with mouse p50$_{cdc37}$ full length as an expression chaperone for protein expression in baculovirus infected Sf9 insect cells. An N-terminal 6x-His tag was inserted into the plasmid, and this plasmid was used as a template to create mutant B-Raf^{V600E}. Site-directed mutagenesis was performed using the manufacturer's protocols (Stratagene) to introduce mutations.

GST-tagged B-Raf^{16mut} and B-Raf^{15mut} proteins were expressed in BL21(DE3)RIL cells at 37 °C,

induced with 1mM IPTG overnight at 16 °C, spun down the next day, and lysed in lysis buffer (50 mM potassium phosphate pH 7.0, 250 mM NaCl, DNase I, 1 mM PMSF). The lysate was spun down at 19,000 rpm for 30 minutes and the supernatant was incubated with GST-Bind resin (Millipore) at 4 °C for 1 hr. The protein on the resin was washed with wash buffer (50 mM potassium phosphate pH 7.0, 250 mM NaCl) overnight and eluted the next morning in wash buffer with 20 mM glutathione and 5 mM βME. The protein was concentrated using a 30kDa cutoff centrifugal filter unit (Millipore) and chromatographed on a Superdex 200 increase column in a final buffer of 20 mM HEPES pH 7.0, 150 mM NaCl, 5% glycerol and 5 mM βME. Protein eluted as a mixture of dimer and monomer and both species were pooled together, concentrated and flash frozen in liquid nitrogen. For certain experiments, the GST-tag was cleaved off. To do this, the protein was not eluted off the GST-Bind resin. Instead, TEV protease was added to the column and incubated overnight at 4 °C. The next morning, the cleaved protein was washed off with 50 mM potassium phosphate pH 7.0, 25 mM NaCl and run over both SP Sepharose and Q Sepharose ion exchange columns in tandem and the flow through was collected. The protein was then concentrated using a 10kDa cutoff centrifugal filter unit (Millipore) and chromatographed on a Superdex S200 gel filtration column in a final buffer of 20 mM HEPES pH 7.0, 150 mM NaCl, 10 mM DTT and 5% glycerol. Protein eluted as a mix of dimer and monomer and both species were pooled together, concentrated and flash frozen in liquid nitrogen.

His-tagged B-Raf was expressed in insect cells essentially as previously described [22]. Briefly, protein constructs were coexpressed with $p50_{cdc37}$, pelleted, suspended in lysis buffer 2 (25 mM pH Tris 8.0, 250 mM NaCl, 5 mM imidazole, and 10% glycerol) treated with Complete EDTA-

free protease inhibitor cocktail tablets (Roche) and DNaseI. After lysis, cell lysates were centrifuged at 19,000 rpm and then incubated with TALON metal affinity resin for 1 hr at 4 °C. The resin was then washed extensively with lysis buffer 2 and the protein was eluted with 25 mM Tris pH 7.5, 250 mM NaCl, 250 mM imidazole, and 10% glycerol. The protein was then diluted in low salt buffer containing 1 mM EDTA and 1 mM DTT before being run on an SP Sepharose column. The protein was eluted with a salt gradient from 0 mM NaCl to 1 M NaCl. Peak fractions were pooled and run on a Superdex s200 gel filtration column and stored in a final buffer of 25 mM Tris pH 8.0, 300 mM NaCl, 1 mM DTT and 10% glycerol. Protein was concentrated to ~0.5mg/mL and flash frozen in liquid nitrogen.

A cDNA library for full length MEK was purchased from Dharmacon (Catalog # MHS 6278-211690391). Full length human MEK1 was cloned into a Pet28a(+) vector encoding an N-terminal 6x-His tag and a TEV protease cleavage site between the tag and protein. Full length human MEK1 with an N-terminal GST fusion tag and a C-terminal His tag in a pGex-3t vector was provided by Dr. Michael Olson (Beatson Institute for Cancer Research, Glasgow, UK).

MEK with an N-terminal 6x-His tag was expressed in DE(3) RIL bacterial expression cells at 37 °C, induced with 1 mM IPTG overnight at 16 °C, spun down the next day, and lysed in lysis buffer 3 (25 mM Tris pH 7.5, 500 mM NaCl, 5 mM βME) supplemented with 1 mM PMSF and DNase I. The lysate was spun down at 19,000 rpm for 30 minutes and the supernatant was added to 10 mL of Ni-NTA metal affinity resin (Thermo Scientific) and left to incubate at 4 °C for 1 hr. The supernatant was then eluted via gravity column and the resin was washed with lysis buffer 3 supplemented with 20 mM imidazole. The MEK protein was eluted with lysis buffer 3

supplemented with 300 mM imidazole. The eluent was dialyzed into dialysis buffer (25 mM Tris pH 7.5, 25 mM NaCl, 5 mM βME) overnight and then applied to a 5 mL Q Sepharose cation exchange column followed by washing in dialysis buffer and elution in 25 mM Tris pH 7.5, 5 mM βME, and 1 M NaCl. Peak fractions were run on an SDS-PAGE gel, pooled, concentrated using a 30k Dalton cutoff centrifugal filter unit (Millipore), and applied to a Superdex 200 increase column in a buffer of 20 mM HEPES pH 7.0, 150 mM NaCl, 5% glycerol and 5 mM βME. Protein was concentrated, flash frozen in liquid nitrogen, and stored at -80 °C.

GST-MEK1 fusion protein used as substrate in ELISA assays was prepared essentially as previously described [22]. Briefly, protein was expressed in BL21(DE3)RIL cells at 37 °C and induced with 0.5 mM IPTG at 15 °C overnight. The cells were then harvested and resuspended in lysis buffer 4 (20 mM HEPES pH 7.5, 500 mM NaCl, 10 mM BME, 10 mM imidazole, 5% glycerol) supplemented with 1 mM PMSF and DNase I. The lysate was sonicated and spun down, and the supernatant was added to Ni-NTA resin and incubated for 1 hr at 4 °C. The resin was then washed extensively with lysis buffer 4 and eluted with lysis buffer 4 supplemented with 250 mM imidazole. Peak fractions were then concentrated using a 50k Dalton cutoff centrifugal filter unit (Millipore) and loaded onto a Superdex s200 gel filtration column in a final buffer of 20 mM HEPES pH 7.0, 150 mM NaCl, 10 mM BME, and 5% glycerol. The protein eluted off the sizing column in two separate populations, and the second peak corresponding to a GST-MEK dimer was collected, concentrated to ~14 mg/mL, flash frozen in liquid nitrogen and stored at -80 °C.

pGEX6P1-GST-HA-ERK2^{K54} was provided by Donita Brady (University of Pennsylvania). GST-ERK2^{K54R} was expressed in DE(3) RIL cells in TB (Dot Scientific) at 37 °C until reaching an OD_{600} of 0.700 and then induced with 1 mM IPTG overnight at 17 °C. The cells were then spun down the next day and lysed in lysis buffer 5 (25 mM Tris pH 7.5, 500 mM NaCl, and 5 mM βME) treated with 1 mM PMSF and DNaseI. The lysate was then spun down at 19,000 rpm for 40 minutes and the supernatant was added to 10 mL of Pierce Glutathione Agarose Resin (product # 16102BID) previously washed with lysis buffer 5 and left to incubate at 4 °C for 2 hr. The supernatant was eluted via gravity column and the resin was then washed with 1 L of lysis buffer 5. The protein was then eluted with lysis buffer 5 supplemented with 20 mM glutathione (Sigma Aldrich, product # G4521) and the elution fractions were pooled together and dialyzed into dialysis buffer (25 mM Tris pH 7.5, 150 mM NaCl, 5 mM βME). The protein was then concentrated and applied to a Superdex S200 10/300 gel filtration column in a final buffer of 25 mM Tris pH 7.5, 150 mM NaCl, 5 mM βME. Protein was concentrated, flash frozen in liquid nitrogen, and stored at -80 °C for future use.

Biolayer Interferometry

Kinetic measurements of mutant GST-B-Raf binding to full length MEK were carried out using the fortéBIO BLItz instrument. After an initial baseline in 20 mM HEPES pH 7.0, 150 mM NaCl, 5% glycerol and 5 mM βME, MEK at a concentration of 0.2 mg/mL was immobilized on Dip and Read™ Ni-NTA Biosensors until saturation was reached (2.5 min). B-Raf constructs were tested at concentrations ranging from 0.25 μM to 20 μM, depending on the particular construct used and its solubility, as well as based on its binding affinity to MEK. Association and dissociation were each monitored for 3 minutes. Step corrections, at the start of association and

at the start of dissociation, were performed manually using Microsoft Excel. Analyses were then performed using a global fit of at least three measurements using nonlinear regression curve fitting in GraphPad Prism, version 8.

Pull Downs

20 μg of GST-B-Raf was incubated with 40 μL of GST-bind resin in a buffer of 20 mM HEPES pH 7.0, 150 mM NaCl, 5 mM βME, and 0.05% Tween 20 for 15 minutes at 4 °C with gentle agitation. Then, an equimolar amount of full length MEK was added and incubated at 4 °C for one hour with gentle agitation. The beads were then washed three times with 1 mL buffer and subjected to SDS-PAGE analysis.

Western Blotting Based Kinase Assay

Reactions were set up with 1 mM ATP and kinase buffer (100 mM Tris, pH 7.5, 10 mM $MgCl_2$ and 5 mM βME) and the indicated kinases. Final concentrations of 50 nM, 200 nM and 200 nM were used for B-Raf, MEK and ERK, respectively. Kinases were diluted in 20 mM HEPES pH 7.0, 150 mM NaCl, 5% glycerol and 5 mM βME prior to addition to reaction mixtures. Phosphorylated MEK and ERK were produced by incubating the enzymes with ATP for 15 and 30 min at 4 °C. In preliminary experiments, it was determined that 15 minutes was more than sufficient to yield complete activation.

Reactions were quenched with 4x loading dye, subjected to SDS-PAGE and then transferred to nitrocellulose membrane to be visualized by western blotting. Membranes were blocked with 5% (w/v) nonfat milk overnight at 4 °C with gentle rocking. The membranes were then incubated

overnight at 4°C with either rabbit anti-p-MEK antibody against Ser217/Ser221 (1:1000) (Cell Signaling, #9121), rabbit anti-p-ERK antibody against Thr202/Tyr204 (1:1000) (Cell Signaling, #9101), anti-MEK antibody (1:1000) (Cell Signaling, #9122), anti-ERK antibody (1:1000) (Cell Signaling, #9102), or anti-GST antibody (1:1000) (Cell Signaling, #2625). The next day, the membranes were incubated with goat anti-rabbit antibody conjugated to HRP (1:500 or 1:1000 against MEK or ERK/GST, respectively) (BioRad) for one hour at room temperature. Bands were visualized by incubating with a solution containing the HRP substrate, 4CN, a color developing solution, following the manufacturer's protocol. Quantitative analyses of the immunoblots were executed with ImageJ software.

ELISA Assay

Kinetics of kinase activity of different constructs (Sf9 expressed His-B-Raf V600E mutant and *E. coli* expressed B-Raf^{15mut}) were determined using an assay modified from that previously described [22]. Briefly, GST-MEK fusion protein was diluted 3:1000 in Tris-Buffered Saline treated with 0.05% Tween 20 (TBST) and diluted MEK was added to a glutathione-coated 96 well plate (Pierce #15240) and incubated at room temperature for 1 hour with shaking. Two rows of the plate were used to generate a standard curve to determine p-MEK product. B-Raf was diluted to 25 nM (or serial dilutions were performed to evaluate enzyme concentration dependence) in 50 mM HEPES pH 7.0 and 50 mM NaCl. Glutathione plates were washed extensively, and 50 μL of protein solution was then added to the plate with 50 μL of ATP solution (200 μM ATP or varied ATP concentration to assess K_m and k_{cat}) in a buffer containing 50 mM HEPES pH 7.0, 200 mM NaCl, and 20 mM $MgCl_2$. The plate was then incubated at RT for 30 minutes to assess concentration of enzyme dependence, for 15 minutes to assess K_m and

k_{cat}, or quenched with 100 mM EDTA at various time points to determine dependence on reaction time. The reaction was then discarded, and the plate was extensively washed with TBST + 100 mM EDTA and a 1:8,000 dilution of primary antibody (p-MEK1/2 (S217/S221) Rabbit Antibody (Cell Signaling)) was added to the plate and incubated for 1 hour. The plate was then washed with TBST and then incubated with a 1:10,000 dilution of secondary antibody (Goat Anti-Rabbit IgG (H+L)-HRP (BioRad)) for 1 hour. The plate was then washed three times and Supersignal ELISA Pico Chemiluminescent Substrate (Pierce #37069) was added and the plate was read on Promega GloMAX 96 Microplate Luminometer. Each curve was repeated in triplicate, using the standard curve to determine product of reactions, and GraphPad Prism 5.0 was used to plot and fit with the model Enzyme kinetics – k_{cat} in the Analyze menu.

Results

Restoration of MEK Complex Formation with the Solubilized *E. coli* Construct of B-Raf

The 16 solubilizing mutations introduced into B-Raf (B-Raf^{16mut}) for bacterial expression are located on the surface of the C-lobe of the kinase domain (Figure 1A, 1B). Interestingly, the combination of these mutations rendered B-Raf inactive, even with the V600E mutation, as it was unable to bind to and phosphorylate MEK. Analysis of the B-Raf-MEK complex structure [8] revealed that the Phe at position 667 could make a key hydrophobic interaction with MEK, and therefore the solubilizing mutation to Glu could have led to charge-charge repulsion with the acidic patch of MEK in which D315 resides (Figure 1C). To test this hypothesis, we generated a mutant in which E667 was reverted back to Phe (B-Raf^{15mut}) for binding and activity assays. This mutant was expressed in *E. coli* with either a 6x-His or GST tag. The size-exclusion

chromatography (SEC) elution profile of the GST-tagged B-Raf^{15mut} (MW ~60kDa) showed two peaks (Figure 2). SDS-PAGE analysis demonstrated that both peaks contain B-Raf; however, absorbance readings demonstrate a high 260/280nm ratio for the first peak. Together with a comparison to standards, this suggests that the first peak contained aggregates. Moreover, the second peak has minimal contamination of other proteins and has dimeric B-Raf, so fractions from this peak were kept for further analysis.

To assess the ability of B-Raf^{15mut} to bind MEK, we performed pull-downs. GST-B-Raf was immobilized on beads and binding of full length, wild-type MEK was visualized using SDS-PAGE. Leaving E667 in the *E. coli* construct ablates complex formation between B-Raf^{16mut} and MEK, whereas the E667F reversion restored B-Raf-MEK complex formation *in vitro* (Figure 3A). We further demonstrated this using biolayer interferometry (BLI) in which MEK was immobilized and binding of GST-B-Raf was tested (Figure 3B). Consistent with the results from pull-downs, no binding of GST-B-Raf^{16mut} was detected, but GST-B-Raf^{15mut} binding to MEK could be detected with a K_D of ~32 nM (Table 1).

MEK can be Phosphorylated by B-Raf^{15mut}

Given that B-Raf^{15mut} could bind to MEK, and because different expression systems could generate proteins with distinct post-translational modifications and therefore distinct activity levels, we next wanted to determine if B-Raf^{15mut} could phosphorylate MEK, its downstream target, and if it does so to the same extent and reaction kinetics as B-Raf^{V600E} produced in Sf9 insect cells. To test this, we incubated untagged B-Raf^{15mut} or 6x-His tagged B-Raf^{V600E} together with MEK and ATP and probed for phosphorylation at Ser218/222 after 15 and 30 minutes

(Figure 3C). This revealed a higher level of phosphorylated MEK by the B-Raf^{V600E} produced in Sf9 insect cells. We then used an ELISA assay for a quantitative analysis of the kinase activities of these two B-Raf constructs. We first determined steady state conditions where the reaction rate is linear versus reaction time and enzyme concentration for each B-Raf we tested (Figure 4A, 4B, 4D and 4E). We chose to work with B-Raf at a concentration of 25 nM and a reaction time of 15 minutes to follow steady-state kinetics. While the k_{cat} values for B-Raf^{V600E} and B-Raf^{15mut} were similar, the K_m values for ATP differed by a factor of ~50. The K_m of B-Raf^{15mut} for ATP was measured to be 27.81 ± 6.64 μM (Figure 4C) and of B-Raf^{V600E} for ATP was 0.57 ± 0.17 μM (Figure 4F). These studies revealed robust B-Raf^{15mut} phosphorylation activity, with apparent Michaelis-Menten kinetics, although at a reduced level relative to B-Raf^{V600E} produced in insect cells. This suggests that while we were able to restore activity of the mutated *E. coli* produced protein, it is not as active as the insect cell-produced B-Raf^{V600E}.

Enhancing MEK Binding to the Solubilized *E. coli* B-Raf Construct

Given that B-Raf^{15mut} was still less active than the B-Raf wild-type counterpart with the V600E mutation, we wanted to determine if there are any other mutations that could enhance the activity of B-Raf^{15mut}. To do this, we further mutated F667 to a Tyr, since we reasoned that this may introduce a hydrogen bond with the nearby D315 and/or N319 of MEK (Figure 5A) while preserving interactions with the MEK hydrophobic pocket, and tested binding by BLI. The introduction of the F667Y mutation in B-Raf^{15mut} enhanced binding affinity to MEK by almost two-fold, due to a reduced dissociation rate of MEK from B-Raf (Figure 5B, Table 1).

A B-Raf α-Helix is Critical for Binding MEK and for MEK Phosphorylation

Reversal of the F667E mutation back to F667 was shown to restore the active state of B-Raf, suggesting an important role for this residue and the α-helix on which it resides in B-Raf-MEK complex formation. Its importance was further demonstrated with the improved binding of B-Raf^{15mut} with the F667Y mutation to MEK (Table 1). The α-helix on which this residue resides reaches into a tunnel in MEK kinase (Figure 6A), so we next wanted to determine if the rest of the α-helix (residues 661-671) is critical for complex formation with MEK. To test this, we generated mutations along this α-helix and determined their effects on MEK binding. Specifically, we produced B-Raf^{15mut} with point mutations N661V, R662E, I666R, and R671A to try to disrupt MEK binding based on the hydrogen bond interactions and complementary electrostatics observed around these residues (Figure 6B-6D). The N661D point mutation was also introduced to try to improve the electrostatic interaction with MEK (Figure 6B).

Each mutant was expressed with a GST-tag in *E. coli* and fractions corresponding to dimer from size exclusion chromatography were isolated. We tested binding by BLI as described above. In agreement with our hypothesis, all mutants tested, except for the non-disruptive N661D mutant, had a higher K_D than the B-Raf^{15mut} construct (Table 1). Of note, the I666R and N661V mutations resulted in the greatest decrease (more than 10-fold) in binding affinity. This decrease was a result of both a slower association rate and an increased dissociation rate.

Given that B-Raf must bind to MEK before phosphorylating it, we next wanted to determine if the mutations in the B-Raf^{15mut} α-helix (residues 661-671) affect its kinase activity. To do this, we used the same *in vitro* phosphorylation assay as described above, but this time using GST-B-Raf constructs. Of all the mutants tested, only B-Raf^{15mut} with the N661V, I666R, or R671A

point mutations showed reduced levels of MEK phosphorylation when compared to B-Raf^{15mut}, and the B-Raf^{15mut} I666R mutant kinase was completely dead (Figure 7). The B-Raf^{15mut} F667Y mutant showed a modest increase in activity under the conditions of the assay. As expected, B-Raf^{16mut} showed negligible activity, and MEK on its own was not able to autophosphorylate, so any phosphorylation observed was due to B-Raf.

B-Raf α-Helix Point Mutations Affect ERK Phosphorylation

Activated MEK goes on to phosphorylate ERK, so we wanted to determine the downstream effects of the B-Raf^{15mut} α-helix mutants. We repeated the same phosphorylation assay and probed for phosphorylation of ERK1 at residues Thr202/Tyr204. Consistent with the levels of MEK phosphorylation observed, ERK phosphorylation was drastically reduced in reaction mixtures that had B-Raf^{15mut} with the N661V, I666R, or R671A point mutations when compared to the reaction mixture in which B-Raf^{15mut} was used. This time, however, we also observed a reduction in ERK phosphorylation in reactions with B-Raf^{15mut} with the R662E mutation. The B-Raf^{15mut} F667Y mutant led to greater downstream ERK phosphorylation under the conditions of the assay. B-Raf^{16mut} led to negligible ERK phosphorylation, as expected, as did MEK without prior phosphorylation by B-Raf^{15mut}. ERK on its own was not able to autophosphorylate, so any phosphorylation observed was due to phosphorylated MEK (Figure 7).

Discussion

A crystal structure of MEK1 in complex with the catalytic domain of wild-type B-Raf was determined by others to help understand B-Raf activity, important for MAPK signaling [8].

Analysis of its structure revealed a residue that had been mutated in the solubilized construct of B-Raf for *E. coli* expression could make an important contact with MEK, thereby affecting its activity [31] (Figure 1B-1C). We showed that this mutation, when reverted to its wild-type residue (F667), restored MEK binding and phosphorylation activity in the *E. coli* construct (Figure 3A-3C, Figure 7). Our phosphorylation assay data revealed that B-Raf^{15mut} produced in *E. coli* had weaker kinase activity than the wild-type B-Raf^{V600E} produced in Sf9 insect cells (Figure 3C, Figure 4). It is possible that the *E. coli* expressed B-Raf^{15mut} was not fully activated, potentially due to different or missing post-translational modifications in the kinase domain when expressed in *E. coli* versus Sf9 insect cells, or the 15 mutations introduced into the bacterially expressed B-Raf^{15mut} also contributed to reducing kinase activity in some other way. Previous reports did not quantify the binding of B-Raf^{16mut} to ATP [31] and so we performed kinetic assays to further characterize B-Raf^{15mut}. Our kinetics data showed that the K_m of B-Raf^{15mut} for ATP was lower than that of B-Raf^{V600E} by a factor of 50 (Figure 4), indicating that the remaining mutations may affect ATP binding and not the ability of B-Raf^{15mut} to bind MEK. This is consistent with our finding that B-Raf^{15mut} had a similar K_D in binding MEK (~32 nM) (Table 1) as the wild-type B-Raf kinase that was expressed in insect cells and used to determine the crystal structure (K_D ~43 nM) [8]. Since the F667Y mutation, introduced into B-Raf^{15mut} to further activate the enzyme, is away from the ATP-binding site, we do not think the B-Raf^{15mut} F667Y mutant would reach the same level of activity as B-Raf^{V600E}. Exploring additional reversion mutations could identify other residues that might improve B-Raf^{15mut} activity. While a lower level of activity from our *E. coli* B-Raf^{15mut} was observed, it is still sufficient for studying the physiological functions of Raf, particularly its interactions and phosphorylation of MEK and downstream effects on ERK. Our

mutant, which can be expressed in *E. coli*, would also be useful for studies requiring large-scale protein preparations, such as those needed for drug screening efforts.

While current B-Raf inhibitors successfully prevent the progression of B-Raf^{V600E}-related cancers for some time, inhibitor resistance and paradoxical activation can occur [25]. Thus, we sought to explore a region of B-Raf that could be used as a drug target for disrupting B-Raf-MEK interactions. B-Raf residue F667, which we demonstrated is important for binding to and phosphorylation of MEK (Figure 5, Table 1), resides on an α-helix that makes extensive interactions with MEK (Figure 6A). We probed the importance of this α-helix by introducing mutations to alter binding to MEK. N661 appears to hydrogen bond with R234 of MEK and mutation to a hydrophobic residue (Val) would eliminate this interaction (Figure 6C). Mutation to Asp, however, could either improve binding by the introduction of a salt bridge, or maintain the same interaction as N661. R662 contacts an acidic patch of MEK, so its charge reversal to Glu would result in charge repulsion (Figure 6B). Similarly, I666 sits near a hydrophobic patch of MEK, so introducing a charged residue (Arg) would lead to an unfavorable interaction (Figure 6B). Finally, R671 appears to hydrogen bond with D315 of MEK, so its mutation to Ala would disrupt this interaction (Figure 6D). Our binding data obtained by BLI is consistent with these hypotheses since the binding affinity was reduced for all mutants predicted to disrupt binding (N661V, R662E, I666R, and R671A). In the case of the N661D mutation, binding to MEK was not affected, suggesting that the mutation to Asp maintains the hydrogen bond with R234 of MEK (Figure 6C). The F667Y mutation, however, was introduced to increase binding and activity, which we observed (Figure 5B, Figure 7, Table 1). In addition to identifying a new target for drug discovery, the various interactions we highlight between the B-Raf α-helix

(residues 661-671) and MEK might suggest useful properties (e.g. charges, hydrogen bond partners, and/or hydrophobic interactions) to take into account when designing inhibitors against this site.

Our *in vitro* phosphorylation assays are consistent with our binding data (Figure 7). While some of the effects were not directly observed when probing for MEK phosphorylation, as in the case of the B-Raf^{15mut} R662E mutant, it could be that the reaction time allowed even weaker MEK binders to complete phosphorylation. The effects of decreased activity of the B-Raf^{15mut} R662E mutant were, however, apparent when probing for phosphorylated ERK. Our results suggest that the B-Raf-MEK α-helix (residues 661-671) interface is a promising target for drug discovery, as it is a different site from current B-Raf inhibitors. Targeting this site could lead to treatments against both B-Raf and B-Raf^{V600E}-induced malignancies, and provide the option of developing combination therapies with ATP-competitive inhibitors to prevent the development of resistance.

Corresponding Author

Email: dfera1@swarthmore.edu, phone: (610) 690-3308

Acknowledgements

D.F. acknowledges support from Swarthmore College Startup and Faculty Research Funds, R.M. acknowledges support from NIH grant CA226888, and L.A.A. acknowledges support from NIH grant CA226888-S1.

Abbreviations

MAPK, mitogen-activated protein kinase; ATP, adenosine triphosphate; GTP, guanosine triphosphate; DTT, dithiothreitol; ELISA, enzyme-linked immunosorbent assay; FPLC, fast protein liquid chromatography; SEC, size exclusion chromatography

Figure Legends

Figure 1. B-Raf-MEK Complex. (a) Sequence alignments of B-Raf kinase domain C-lobe. Mutations in the solubilized construct are shown in red. Mutations introduced in this study are shown with various symbols. Conserved residues with respect to wild-type B-Raf with the V600E mutation are marked by an asterisk below the alignment. (b) Structure of the B-Raf-MEK complex. The two proteins are shown as cartoons with the B-Raf N-lobe in pink, B-Raf C-lobe in purple, MEK N-lobe in blue, and MEK C-lobe in cyan. The residue that was mutated to produce active B-Raf with 15 surface mutations is shown in sticks and highlighted with a red star. The α-helix under study is indicated. Figure generated using PDB ID: 4MNE. (c) Zoomed in view of the B-Raf α-helix. The α-helix is shown as a purple cartoon with the solubilizing mutation that interacts with MEK shown as sticks. The electrostatic surface potential of the MEK C-lobe is shown (blue is positively charged and red is negatively charged) and the position of D315 is shown with a cyan star. Figure generated using PDB ID: 4MNE.

Figure 2. Purification of GST-B-Raf^{15mut} from *E. coli*. (a) FPLC trace of size-exclusion chromatography run of GST-B-Raf^{15mut}. The elution volumes of protein standards (158 and 44 kDa) are indicated by arrows. (b) SDS-PAGE analysis of fractions from the corresponding size-

exclusion chromatography run. Fraction numbers are indicated and those kept for analysis are boxed.

Figure 3. Binding and activity of B-Raf^{15mut}. (a) SDS-PAGE gel of pull-down assay of GST-B-Raf^{16mut} or GST-B-Raf^{15mut} with full length MEK^{WT}. The MEK band is indicated with a red star. (b) BLI curves of GST-B-Raf^{16mut} and GST-B-Raf^{15mut} binding to full length MEK^{WT}. In each case, His-tagged MEK^{WT} was immobilized onto an anti-His biosensor, and B-Raf constructs were introduced at two or more concentrations, ranging from low micromolar to high micromolar, depending on the mutant tested. Global fits are shown as black lines. (c) Western blot for *in vitro* phosphorylation of MEK^{WT} using B-Raf^{V600E} expressed in Sf9 cells compared to B-Raf^{15mut} expressed in *E. coli*.

Figure 4. Enzymatic characterization of B-Raf^{15mut} and B-Raf^{V600E}. The kinase activity of B-Raf^{15mut} is linear versus (a) reaction time and (b) enzyme concentration (c) Steady-state kinetic analysis of B-Raf^{15mut}. K_m for ATP and k_{cat} were obtained with varying concentrations of ATP. The kinase activity of B-Raf^{V600E} is linear versus (d) reaction time and (e) enzyme concentration (f) Steady-state kinetic analysis of B-Raf^{V600E}. K_m for ATP and k_{cat} were obtained with varying concentrations of ATP.

Figure 5. Improving B-Raf binding to MEK. (a) The introduced B-Raf Y667 mutation is shown as purple sticks and its possible interactions with MEK residues (cyan) are shown. Hydrogen bond distances are shown with dashed lines and distances are provided. Figure generated using PDB ID: 4MNE. (b) Representative BLI curves of the GST-B-Raf^{15mut} F667Y

mutant binding to immobilized full length His-tagged MEK^{WT}. B-Raf was introduced at the indicated concentrations. Global fits are shown as black lines.

Figure 6. Interactions of B-Raf α-helix with the MEK C-lobe. (a) The B-Raf α-helix under study is shown as a purple cartoon with residues mutated in this study shown as sticks. The MEK C-lobe is shown as a cyan surface and electrostatics surface (b). (c) The potential interaction of the B-Raf residue N661 with the indicated MEK residue shown as sticks. (d) The potential interaction of the B-Raf residue R671 with the indicated MEK residue shown as sticks. Hydrogen bonds and salt-bridges are shown with dashed lines and distances are provided. Figure generated using PDB ID: 4MNE.

Figure 7. *In vitro* Phosphorylation of MEK and ERK by B-Raf^{15mut} α-helix mutants. MEK and ERK were incubated with ATP with or without the indicated constructs of B-Raf for 30 minutes. Reaction mixtures were subjected to Western blot analysis with anti-p-MEK and anti-p-ERK antibodies. Input lanes are shown in blue. B-Raf and ERK were both GST-tagged. The intensities of the p-MEK and p-ERK were quantified by ImageJ and normalized to the corresponding band from the mixture with B-Raf^{15mut}.

References

[1] Burotto, M., Chiou, V. L., Lee, J. M., and Kohn, E. C. (2014) The MAPK pathway across different malignancies: a new perspective, *Cancer 120*, 3446-3456.

[2] Dhillon, A. S., Hagan, S., Rath, O., and Kolch, W. (2007) MAP kinase signalling pathways in cancer, *Oncogene 26*, 3279-3290.

[3] Murphy, L. O., and Blenis, J. (2006) MAPK signal specificity: the right place at the right time, *Trends Biochem Sci 31*, 268-275.

[4] Lowy, D. R., and Willumsen, B. M. (1993) Function and regulation of ras, *Annu Rev Biochem 62*, 851-891.

[5] Vojtek, A. B., and Der, C. J. (1998) Increasing complexity of the Ras signaling pathway, *J Biol Chem 273*, 19925-19928.

[6] Moelling, K., Heimann, B., Beimling, P., Rapp, U. R., and Sander, T. (1984) Serine- and threonine-specific protein kinase activities of purified gag-mil and gag-raf proteins, *Nature 312*, 558-561.

[7] Shaw, A. S., Kornev, A. P., Hu, J., Ahuja, L. G., and Taylor, S. S. (2014) Kinases and pseudokinases: lessons from RAF, *Mol Cell Biol 34*, 1538-1546.

[8] Haling, J. R., Sudhamsu, J., Yen, I., Sideris, S., Sandoval, W., Phung, W., Bravo, B. J., Giannetti, A. M., Peck, A., Masselot, A., Morales, T., Smith, D., Brandhuber, B. J., Hymowitz, S. G., and Malek, S. (2014) Structure of the BRAF-MEK complex reveals a kinase activity independent role for BRAF in MAPK signaling, *Cancer Cell 26*, 402-413.

[9] Zhang, W., and Liu, H. T. (2002) MAPK signal pathways in the regulation of cell proliferation in mammalian cells, *Cell Res 12*, 9-18.

[10] Ascierto, P. A., Kirkwood, J. M., Grob, J. J., Simeone, E., Grimaldi, A. M., Maio, M., Palmieri, G., Testori, A., Marincola, F. M., and Mozzillo, N. (2012) The role of BRAF V600 mutation in melanoma, *J Transl Med 10*, 85.

[11] Davies, H., Bignell, G. R., Cox, C., Stephens, P., Edkins, S., Clegg, S., Teague, J., Woffendin, H., Garnett, M. J., Bottomley, W., Davis, N., Dicks, E., Ewing, R., Floyd, Y., Gray, K., Hall, S., Hawes, R., Hughes, J., Kosmidou, V., Menzies, A., Mould, C., Parker, A., Stevens, C., Watt, S., Hooper, S., Wilson, R., Jayatilake, H., Gusterson, B. A., Cooper, C., Shipley, J., Hargrave, D., Pritchard-Jones, K., Maitland, N., Chenevix-Trench, G., Riggins, G. J., Bigner, D. D., Palmieri, G., Cossu, A., Flanagan, A., Nicholson, A., Ho, J. W., Leung, S. Y., Yuen, S. T., Weber, B. L., Seigler, H. F., Darrow, T. L., Paterson, H., Marais, R., Marshall, C. J., Wooster, R., Stratton, M. R., and Futreal, P. A. (2002) Mutations of the BRAF gene in human cancer, *Nature 417*, 949-954.

[12] Wan, P. T., Garnett, M. J., Roe, S. M., Lee, S., Niculescu-Duvaz, D., Good, V. M., Jones, C. M., Marshall, C. J., Springer, C. J., Barford, D., Marais, R., and Cancer Genome, P.

(2004) Mechanism of activation of the RAF-ERK signaling pathway by oncogenic mutations of B-RAF, *Cell 116*, 855-867.

[13] Pritchard, C. A., Samuels, M. L., Bosch, E., and McMahon, M. (1995) Conditionally oncogenic forms of the A-Raf and B-Raf protein kinases display different biological and biochemical properties in NIH 3T3 cells, *Mol Cell Biol 15*, 6430-6442.

[14] Hu, J., Ahuja, L. G., Meharena, H. S., Kannan, N., Kornev, A. P., Taylor, S. S., and Shaw, A. S. (2015) Kinase regulation by hydrophobic spine assembly in cancer, *Mol Cell Biol 35*, 264-276.

[15] Matallanas, D., Birtwistle, M., Romano, D., Zebisch, A., Rauch, J., von Kriegsheim, A., and Kolch, W. (2011) Raf family kinases: old dogs have learned new tricks, *Genes Cancer 2*, 232-260.

[16] Zheng, C. F., and Guan, K. L. (1994) Activation of MEK family kinases requires phosphorylation of two conserved Ser/Thr residues, *EMBO J 13*, 1123-1131.

[17] Ramos, J. W. (2008) The regulation of extracellular signal-regulated kinase (ERK) in mammalian cells, *Int J Biochem Cell Biol 40*, 2707-2719.

[18] Zhang, J., Zhang, F., Ebert, D., Cobb, M. H., and Goldsmith, E. J. (1995) Activity of the MAP kinase ERK2 is controlled by a flexible surface loop, *Structure 3*, 299-307.

[19] Roberts, P. J., and Der, C. J. (2007) Targeting the Raf-MEK-ERK mitogen-activated protein kinase cascade for the treatment of cancer, *Oncogene 26*, 3291-3310.

[20] Unal, E. B., Uhlitz, F., and Bluthgen, N. (2017) A compendium of ERK targets, *FEBS Lett 591*, 2607-2615.

[21] Sullivan, R. J., and Flaherty, K. T. (2015) New strategies in melanoma: entering the era of combinatorial therapy, *Clin Cancer Res 21*, 2424-2435.

[22] Qin, J., Xie, P., Ventocilla, C., Zhou, G., Vultur, A., Chen, Q., Liu, Q., Herlyn, M., Winkler, J., and Marmorstein, R. (2012) Identification of a novel family of BRAF(V600E) inhibitors, *J Med Chem 55*, 5220-5230.

[23] Dankner, M., Rose, A. A. N., Rajkumar, S., Siegel, P. M., and Watson, I. R. (2018) Classifying BRAF alterations in cancer: new rational therapeutic strategies for actionable mutations, *Oncogene 37*, 3183-3199.

[24] Tran, K. A., Cheng, M. Y., Mitra, A., Ogawa, H., Shi, V. Y., Olney, L. P., Kloxin, A. M., and Maverakis, E. (2016) MEK inhibitors and their potential in the treatment of advanced melanoma: the advantages of combination therapy, *Drug Des Devel Ther 10*, 43-52.

[25] Oh, Y. T., Deng, J., Yue, P., and Sun, S. Y. (2016) Paradoxical activation of MEK/ERK signaling induced by B-Raf inhibition enhances DR5 expression and DR5 activation-induced apoptosis in Ras-mutant cancer cells, *Sci Rep 6*, 26803.

[26] Holderfield, M., Nagel, T. E., and Stuart, D. D. (2014) Mechanism and consequences of RAF kinase activation by small-molecule inhibitors, *Br J Cancer 111*, 640-645.

[27] Griffin, M., Scotto, D., Josephs, D. H., Mele, S., Crescioli, S., Bax, H. J., Pellizzari, G., Wynne, M. D., Nakamura, M., Hoffmann, R. M., Ilieva, K. M., Cheung, A., Spicer, J. F., Papa, S., Lacy, K. E., and Karagiannis, S. N. (2017) BRAF inhibitors: resistance and the promise of combination treatments for melanoma, *Oncotarget 8*, 78174-78192.

[28] Bosch, E., Cherwinski, H., Peterson, D., and McMahon, M. (1997) Mutations of critical amino acids affect the biological and biochemical properties of oncogenic A-Raf and Raf-1, *Oncogene 15*, 1021-1033.

[29] Cope, N., Candelora, C., Wong, K., Kumar, S., Nan, H., Grasso, M., Novak, B., Li, Y., Marmorstein, R., and Wang, Z. (2018) Mechanism of BRAF Activation through Biochemical Characterization of the Recombinant Full-Length Protein, *Chembiochem 19*, 1988-1997.

[30] Park, E., Rawson, S., Li, K., Kim, B. W., Ficarro, S. B., Pino, G. G., Sharif, H., Marto, J. A., Jeon, H., and Eck, M. J. (2019) Architecture of autoinhibited and active BRAF-MEK1-14-3-3 complexes, *Nature 575*, 545-550.

[31] Tsai, J., Lee, J. T., Wang, W., Zhang, J., Cho, H., Mamo, S., Bremer, R., Gillette, S., Kong, J., Haass, N. K., Sproesser, K., Li, L., Smalley, K. S., Fong, D., Zhu, Y. L., Marimuthu, A., Nguyen, H., Lam, B., Liu, J., Cheung, I., Rice, J., Suzuki, Y., Luu, C., Settachatgul, C., Shellooe, R., Cantwell, J., Kim, S. H., Schlessinger, J., Zhang, K. Y., West, B. L., Powell, B., Habets, G., Zhang, C., Ibrahim, P. N., Hirth, P., Artis, D. R., Herlyn, M., and Bollag, G. (2008) Discovery of a selective inhibitor of oncogenic B-Raf kinase with potent antimelanoma activity, *Proc Natl Acad Sci U S A 105*, 3041-3046.

Figure 1

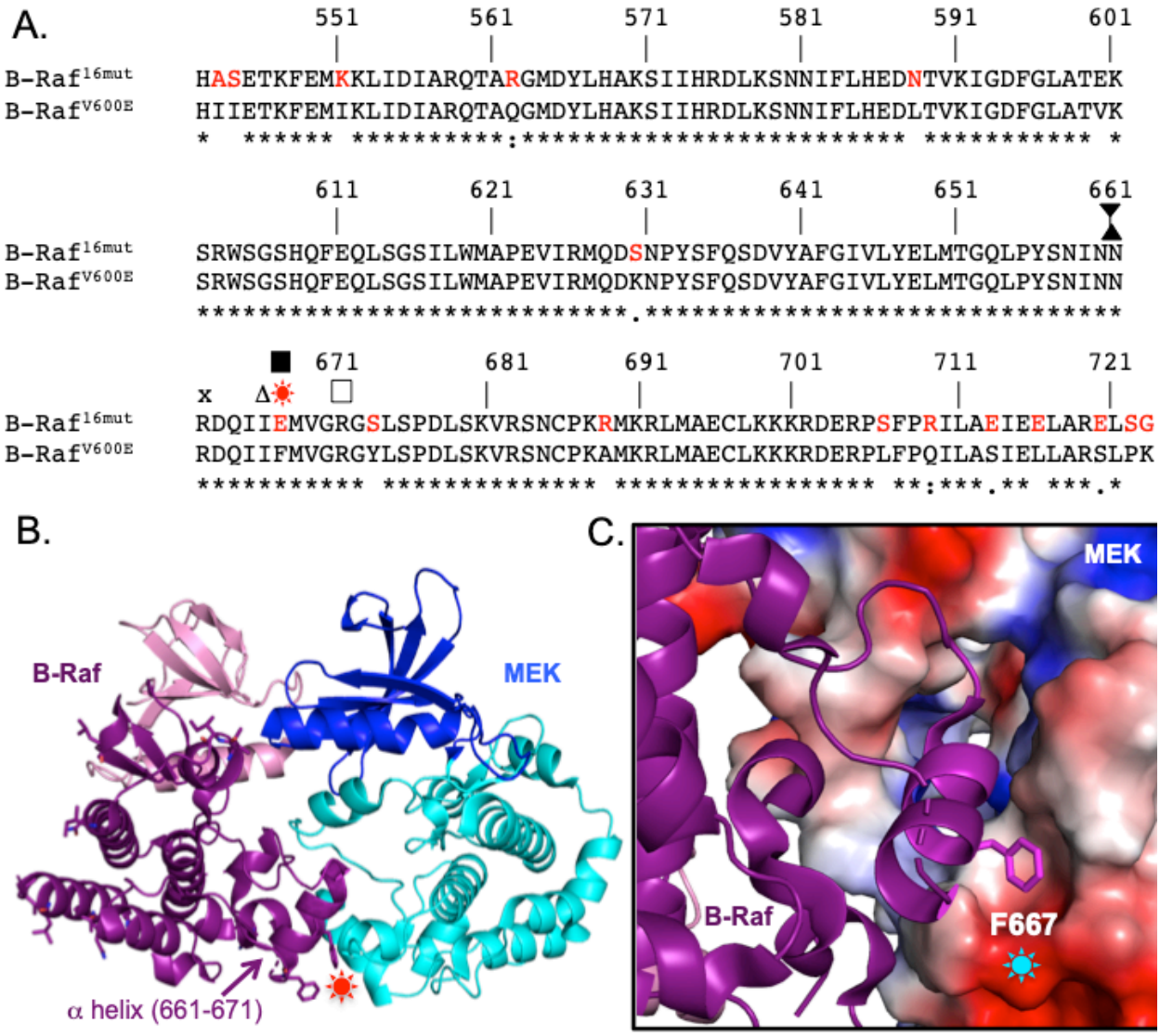
A.
551 561 571 581 591 601
B-Raf16mut HASETKFEMKKLIDIARQTARGMDYLHAKSIIHRDLKSNNIFLHEDNTVKIGDFGLATEK
B-RafV600E HIIETKFEMIKLIDIARQTAQGMDYLHAKSIIHRDLKSNNIFLHEDLTVKIGDFGLATVK
611 621 631 641 651 661
B-Raf16mut SRWSGSHQFEQLSGSILWMAPEVIRMQDSNPYSFQSDVYAFGIVLYELMTGQLPYSNINN
B-RafV600E SRWSGSHQFEQLSGSILWMAPEVIRMQDKNPYSFQSDVYAFGIVLYELMTGQLPYSNINN
671 681 691 701 711 721
x Δ
B-Raf16mut RDQIIEMVGRGSLSPDLSKVRSNCPKRMKRLMAECLKKKRDERPSFPRILAEIEELARELSG
B-RafV600E RDQIIFMVGRGYLSPDLSKVRSNCPKAMKRLMAECLKKKRDERPLFPQILASIELLARSLPK
B.
B-Raf
MEK
α helix (661-671)
C.
MEK
B-Raf
F667

Figure 2

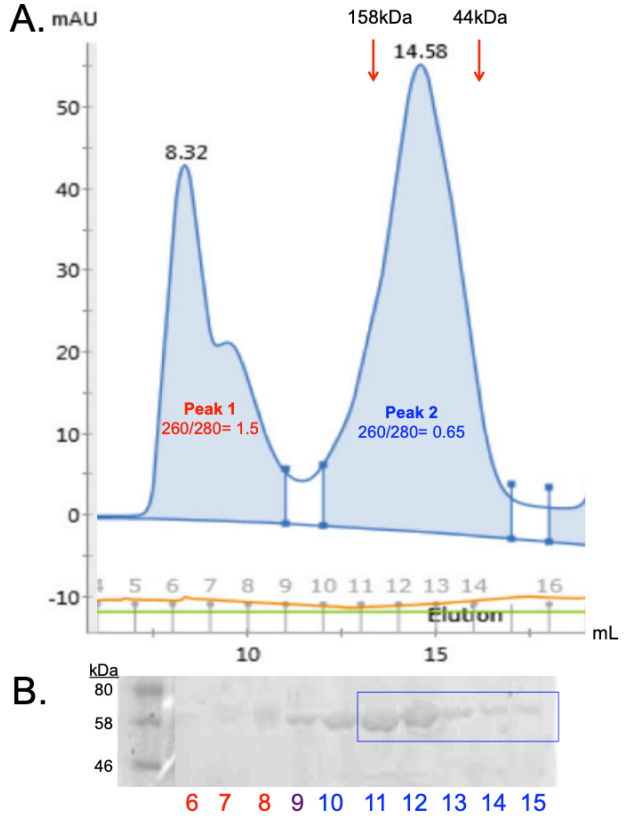
A.
mAU
158kDa
44kDa
14.58
8.32
50
40
30
20
10
0
-10
Peak 1
260/280= 1.5
Peak 2
260/280= 0.65
5 6 7 8 9 10 11 12 13 14 16
Elution
mL
10
15
B.
kDa
80
58
46
6 7 8 9 10 11 12 13 14 15

Figure 3

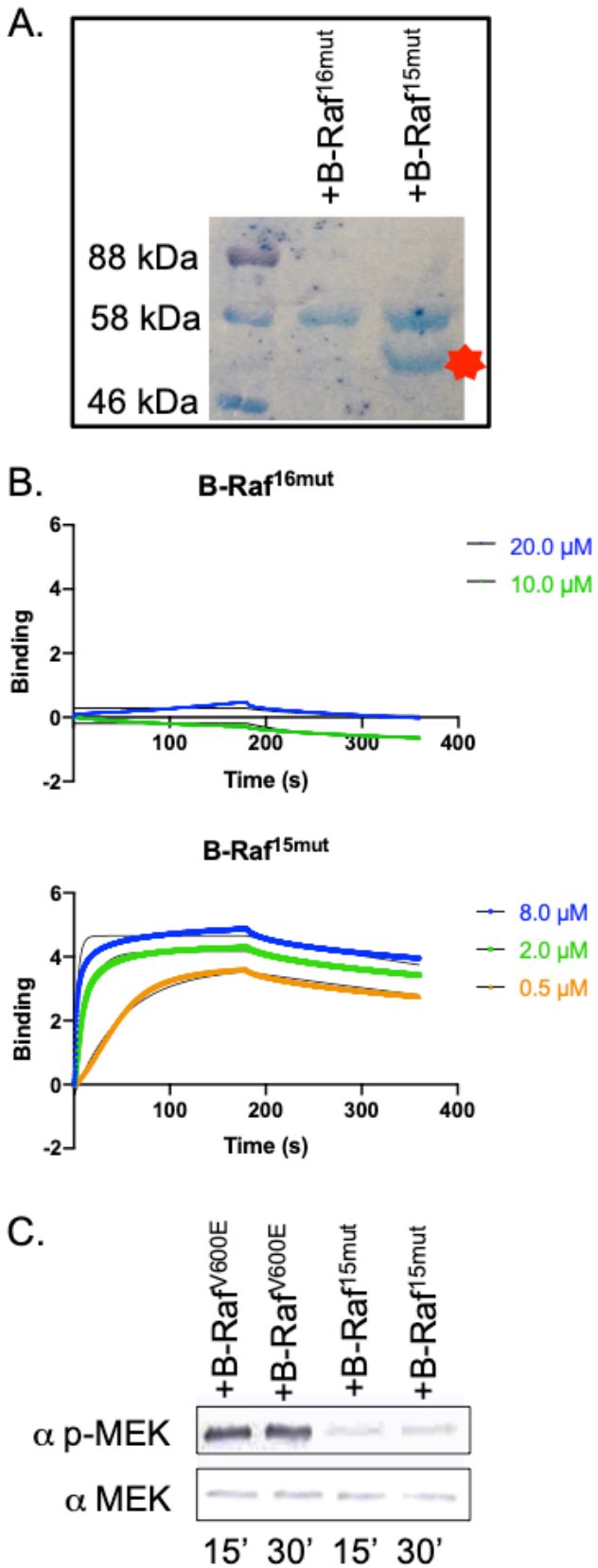
A.
+B-Raf16mut
+B-Raf15mut
88 kDa
58 kDa
46 kDa
B.
B-Raf16mut
20.0 μM
10.0 μM
Binding
Time (s)
B-Raf15mut
8.0 μM
2.0 μM
0.5 μM
Binding
Time (s)
C.
+B-RafV600E
+B-RafV600E
+B-Raf15mut
+B-Raf15mut
α p-MEK
α MEK
15' 30' 15' 30'

Figure 4

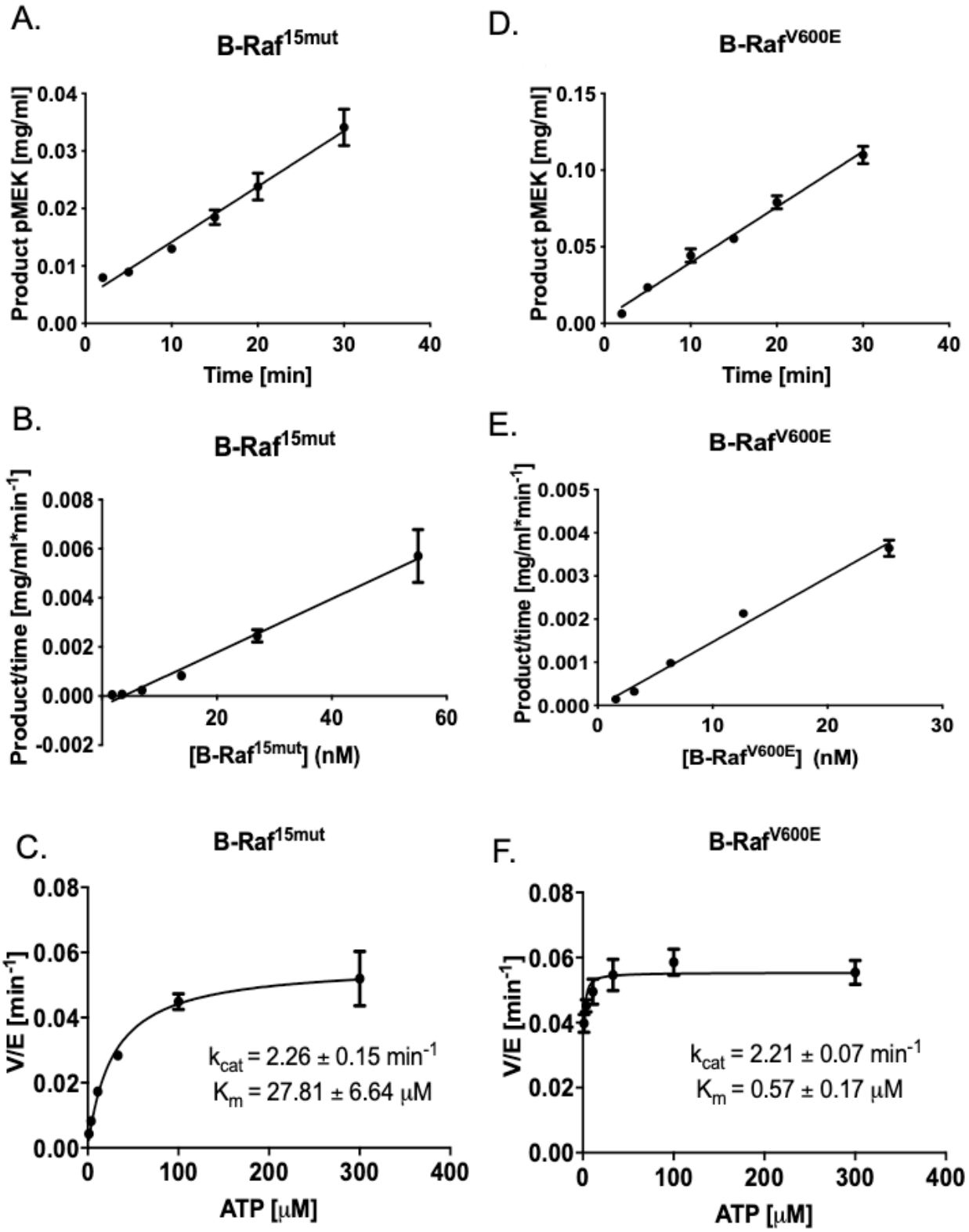
A.
B-Raf15mut
Product pMEK [mg/ml]
Time [min]
D.
B-RafV600E
Product pMEK [mg/ml]
Time [min]
B.
B-Raf15mut
Product/time [mg/ml*min-1]
[B-Raf15mut] (nM)
E.
B-RafV600E
Product/time [mg/ml*min-1]
[B-RafV600E] (nM)
C.
B-Raf15mut
V/E [min-1]
kcat = 2.26 ± 0.15 min-1
Km = 27.81 ± 6.64 μM
ATP [μM]
F.
B-RafV600E
V/E [min-1]
kcat = 2.21 ± 0.07 min-1
Km = 0.57 ± 0.17 μM
ATP [μM]

Figure 5

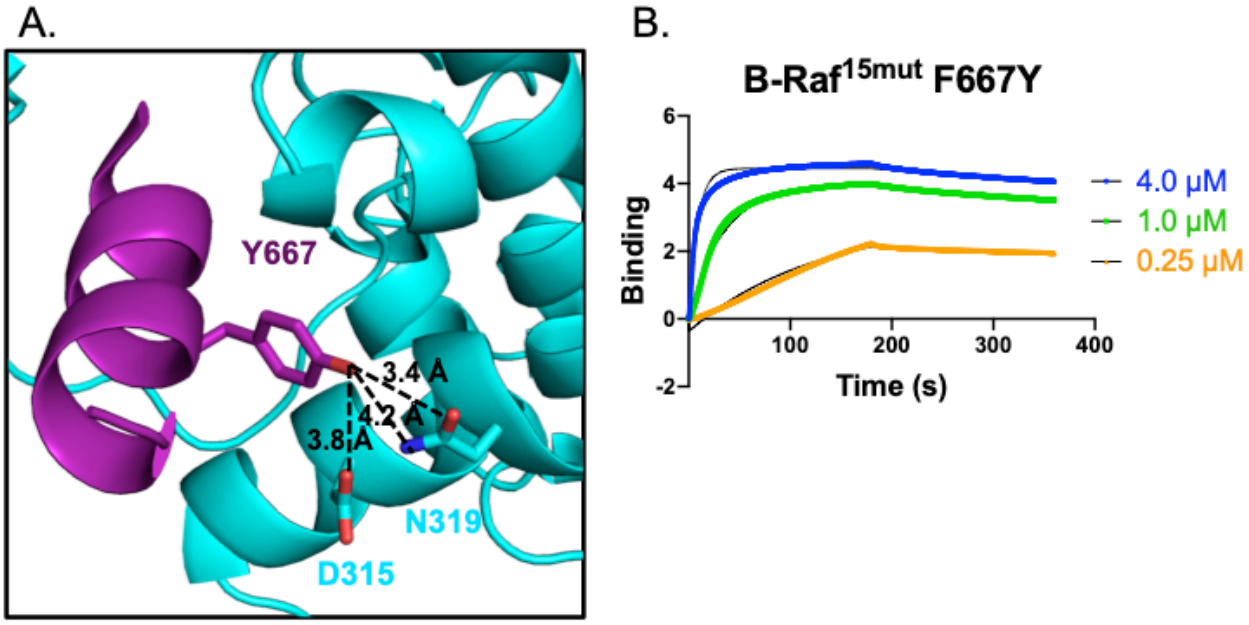
A.
Y667
3.4 Å
4.2 Å
3.8 Å
N319
D315
B.
B-Raf15mut F667Y
Binding
Time (s)
4.0 μM
1.0 μM
0.25 μM

Figure 6

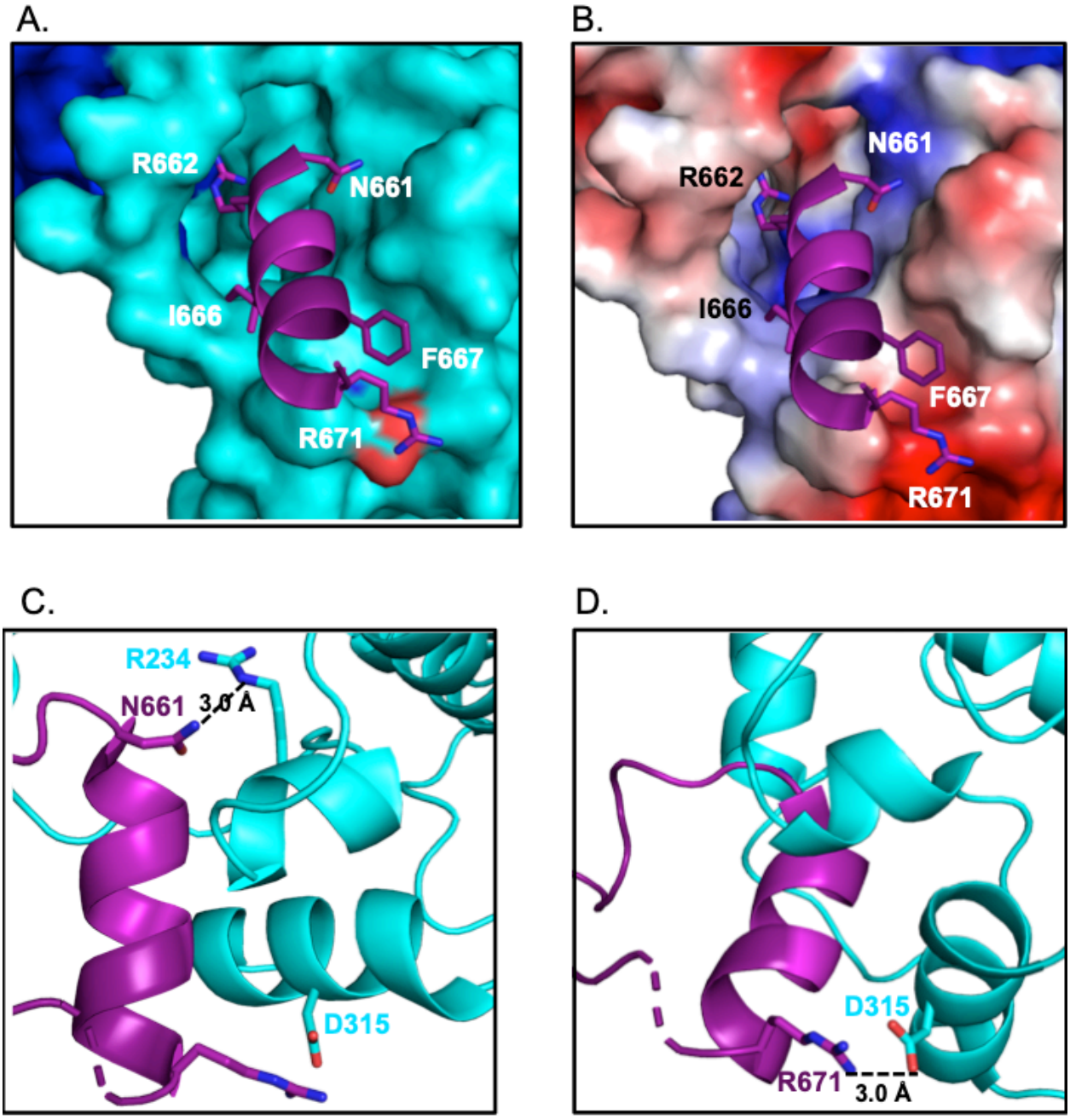
A.
R662
N661
I666
F667
R671
B.
N661
R662
I666
F667
R671
C.
R234
N661
3.0 Å
D315
D.
D315
R671
3.0 Å

Figure 7

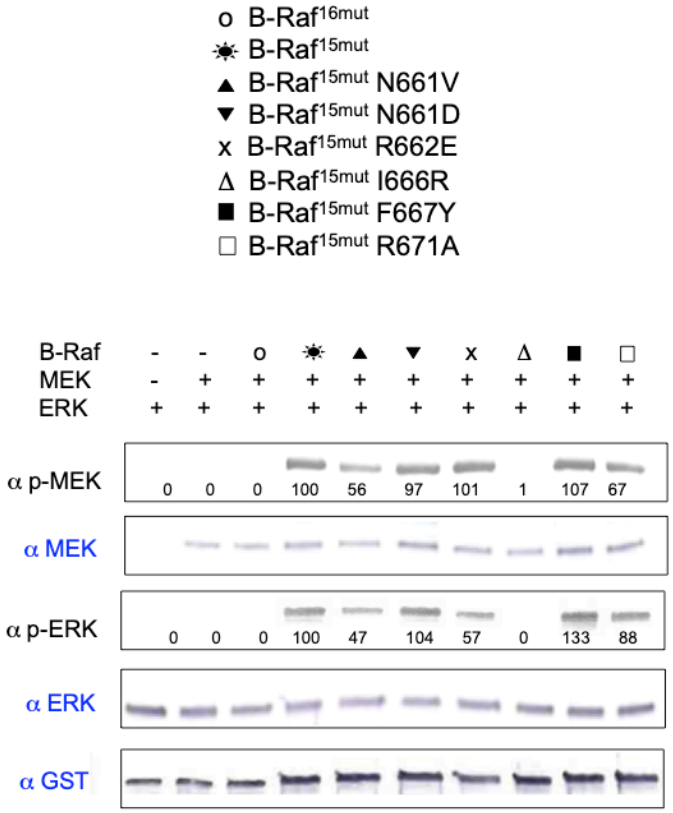
o B-Raf16mut
B-Raf15mut
▲ B-Raf15mut N661V
▼ B-Raf15mut N661D
x B-Raf15mut R662E
Δ B-Raf15mut I666R
■ B-Raf15mut F667Y
□ B-Raf15mut R671A
B-Raf - - o ▲ ▼ x Δ ■ □
MEK - + + + + + + + + +
ERK + + + + + + + + + +
α p-MEK
0 0 0 100 56 97 101 1 107 67
α MEK
α p-ERK
0 0 0 100 47 104 57 0 133 88
α ERK
α GST

Table 1. Equilibrium dissociation constant (K_D) and association and dissociation rate constants (k_{on} and k_{off}) from BLI for indicated B-Raf constructs and full length wild-type MEK

B-Raf^{15mut} mutant	**K_D** (nM)	**k_{on}** ($\times 10^3$ $M^{-1}s^{-1}$)	**k_{off}** ($\times 10^{-3}$ s^{-1})
B-Raf^{16mut}	NB	NB	NB
E667F (B-Raf^{15mut})	32.41 ± 1.34	35.79 ± 0.65	1.16 ± 0.27
N661V	508.10 ± 4.16	5.00 ± 0.28	2.54 ± 0.17
N661D	36.17 ± 1.31	58.89 ± 1.10	2.13 ± 0.04
R662E	160.6 ± 15.13	25.09 ± 1.15	4.03 ±0.17
I666R	985.65 ± 133.35	6.27 ± 0.59	6.18 ± 0.32
F667Y	18.55 ± 0.70	29.64 ± 0.35	0.55 ± 0.01
R671A	47.94 ± 2.16	24.20 ± 0.49	1.16 ± 0.03

NB denotes no binding detected.